NASA Technical Paper 1178

Low-Speed Aerodynamic Performance of 50.8-Centimeter-Diameter Noise-Suppressing Inlets for the Quiet, Clean, Short-Haul Experimental Engine (QCSEE)

John M. Abbott, James H. Diedrich,
and Robert C. Williams

AUGUST 1978

NASA

NASA Technical Paper 1178

Low-Speed Aerodynamic Performance of 50.8-Centimeter-Diameter Noise-Suppressing Inlets for the Quiet, Clean, Short-Haul Experimental Engine (QCSEE)

John M. Abbott, James H. Diedrich,
and Robert C. Williams
Lewis Research Center
Cleveland, Ohio

National Aeronautics
and Space Administration

**Scientific and Technical
Information Office**

1978

LOW-SPEED AERODYNAMIC PERFORMANCE OF 50.8-CENTIMETER-DIAMETER NOISE-SUPPRESSING INLETS FOR THE QUIET, CLEAN, SHORT-HAUL EXPERIMENTAL ENGINE (QCSEE)

by John M. Abbott, James H. Diedrich, and Robert C. Williams

Lewis Research Center

SUMMARY

A series of tests were conducted to determine the aerodynamic performance of inlets designed for the quiet, clean, short-haul, experimental engine (QCSEE). Two basic inlet concepts were tested - a high-throat-Mach-number (0.79) design and a low-throat-Mach-number (0.60) design. Both concepts were tested with four diffuser acoustical treatment designs that had face-sheet porosity ranging from 0 to 24 percent for the high-Mach-number inlet and 0 to 28 percent for the low-Mach-number inlet.

The tests were conducted in a low-speed wind tunnel at free-stream velocities of 0, 41, and 62 meters per second and angles of attack to 50°. Inlet throat Mach number was varied about the design value.

Increasing inlet diffuser face-sheet porosity resulted in an increase in total-pressure loss in the boundary layer for both the high- and low-Mach-number inlet designs. However, the overall effect on inlet total-pressure recovery was insigificant. The primary inlet configuration intended for use with the QCSEE engine (high Mach number, 9.2-percent porosity) had a total-pressure recovery of 0.991 at the design throat Mach number, a free-stream velocity of 41 meters per second, and an angle of attack of 50°.

Inlet flow separation at an angle of attack of 50° was encountered with only one inlet configuration - the high-Mach-number design with the highest diffuser face-sheet porosity (24 percent).

INTRODUCTION

A program is under way at the Lewis Research Center to develop a quiet, clean, short-haul, experimental engine (QCSEE). The quiet and short-haul aspects of this

engine program have placed some particular design requirements on the engine inlet. First, for the engine to be quiet, the inlet must suppress forward-radiated engine noise. Second, for the short-haul aircraft application, the engine inlet, which is ahead of the wing, will be exposed to high upflow angles at takeoff and approach because of the high-lift flow field generated by the wing of a short-haul, powered-lift aircraft (ref. 1).

Two basic inlet acoustical design concepts were considered for inlet noise suppression. The primary inlet design, the high-Mach-number inlet, incorporates the high-throat-Mach-number ($M_t = 0.79$) concept for noise suppression at takeoff (refs. 2 and 3). The inlet diffuser walls are lined with acoustic treatment, which is designed to provide suppression during reverse-thrust operation of the engine. At approach, a somewhat reduced throat Mach number (because of the reduced engine weight flow) in combination with the acoustic treatment provides the noise suppression.

With this high-Mach-number inlet concept, relatively large changes in inlet throat Mach number (and hence noise suppression) can occur for small changes in inlet airflow. Therefore, maintaining a constant level of noise suppression with this inlet concept requires that the QCSEE engine control engine weight flow quite accurately under changing conditions of free-stream velocity and angle of attack. As reported in reference 3 an effective control parameter for maintaining constant inlet-throat Mach number is the ratio of an inlet diffuser surface static pressure to free-stream total pressure. The surface static pressure is measured sufficiently far downstream in the diffuser and also on the side walls of the diffuser in order to eliminate any effect of changes in free-stream velocity and angle of attack on the one-to-one relation between the control parameter and throat Mach number. This control parameter will be used by the QCSEE engine to control inlet weight flow (by adjusting fan-blade pitch angle and fan exit area as required).

The secondary inlet acoustical design concept, the low-Mach-number inlet ($M_t = 0.60$), was developed as a backup should the relatively new concept of a high-Mach-number inlet not perform satisfactorily either aerodynamically or acoustically. In this design, noise suppression at takeoff, approach, and reverse thrust is provided by the acoustically treated inlet diffuser walls.

For each of these two basic inlet concepts, high Mach number and low Mach number, three diffuser acoustical treatment designs were tested, with face-sheet porosity being the main variable. A hard-wall diffuser was also tested for each inlet design, for a total of eight inlet configurations.

The acoustic design goals for both inlet concepts are described in references 4 and 5. From the results presented in these references, the high-Mach-number inlet design with a diffuser face-sheet porosity of 9.2 percent was judged to be the most promising acoustically and was thus selected as the primary QCSEE inlet design from an acoustics standpoint.

The aerodynamic design goals of the inlets are satisfactory inlet performance (1) at

static conditions, (2) at a 50° angle of attack at 41 meters per second (80 knots), and (3) in a 90° crosswind of 18 meters per second (35 knots). A 30.48-centimeter-diameter, high-Mach-number inlet with a hard-wall diffuser was tested previously and satisfactorily met these goals (ref. 6).

This investigation was limited to aerodynamic performance and was conducted (1) to verify that these inlets would perform satisfactorily with acoustical treatment on the diffuser walls (particularly the high-Mach-number inlet with 9.2-percent porosity), (2) to determine the effect of the treatment design on the internal boundary-layer characteristics, and (3) to verify the choice of location for the diffuser static-pressure measurement used to establish the QCSEE engine weight-flow control parameter with the high-Mach-number inlet concept. The inlets were sized to fit a 50.8-centimeter-diameter engine simulator. Data were taken for each inlet at free-stream velocities of 0, 41, and 62 meters per second and angles of attack to 50°. Inlet throat Mach number was varied from 0.33 to 0.82 for the high-Mach-number inlets and from 0.30 to 0.62 for the low-Mach-number inlets.

SYMBOLS

A	area
a	ellipse semimajor axis of internal lip (fig. 4)
b	ellipse semiminor axis of internal lip (fig. 4)
c	external forebody length (fig. 4)
D	diameter
D_{max}	inlet total-pressure-distortion parameter, (Maximum total pressure - Minimum total pressure)/(Average total pressure)
D_{60}	inlet circumferential total-pressure-distortion parameter, (Average total pressure - Minimum average total pressure over any 60° circumferential sector)/(Average total pressure)
d	external forebody thickness (fig. 4)
H	flow-passage height at fan face (fig. 4)
h	radial distance from inlet outer wall (fig. 4)
K	diffuser face-sheet thickness (table II), cm
L	length
M	Mach number

m	diffuser treatment backing depth (table II), cm
n	diffuser face-sheet hole diameter (table II), cm
P	total pressure
P_{0^o}	total pressure measured at rake measuring plane at 0^o circumferential position (fig. 6)
P_{180^o}	total pressure measured at rake measuring plane at 180^o circumferential position (fig. 6)
$(\Delta P/P)_{muff}$	muffler weight-flow parameter defined in fig. 8(b)
$(\Delta P/P)_{0.4}$	high-Mach-number inlet weight-flow control parameter defined in fig. 18
p	static pressure
V	velocity
$\dot{w}$	weight flow
x	axial distance from inlet highlight (fig. 4)
y	radial distance from inlet highlight (fig. 4)
α	angle of attack, deg
δ	ratio of total pressure to standard sea-level pressure
θ	ratio of total temperature to standard sea-level temperature
λ_{max}	maximum diffuser wall angle (fig. 4), deg
ψ	inlet circumferential position, deg
Subscripts:	
av	average
bm	bellmouth
c	centerbody
d	diffuser
e	diffuser exit
f	diffuser face sheet
hl	inlet highlight
inlet	inlet
l	lip
muff	muffler
plug	muffler-exit plug

s	inlet surface
t	inlet throat
turb	simulator turbine
0	free stream
1	rake measuring station (fan face)
2	fan stage exit

APPARATUS

Test Facility and Model

The general arrangement of the test installation in the Lewis 9- by 15-Foot Low-Speed Wind Tunnel (ref. 7) is shown in figure 1. The model installed in the test section is shown in figure 2.

The test inlets were mounted to a 50.8-centimeter-diameter model fan that provided the inlet airflow. A schematic view of the test model is shown in figure 3. The model was mounted on a turntable for testing over a range of angle of attack. The fan was driven by a core turbine powered by high-pressure, heated air delivered to the turbine through flow passages in the support strut. The model exhaust (both fan and turbine) was ducted out of the test section into a rear noise-suppressing muffler. This was done for an inlet acoustic test program that is reported in reference 8. A remotely adjustable plug at the muffler-exit station was used to set the desired fan operating point. Details of the fan operating conditions are given in a following discussion of simulator operation.

Inlet Design

The inlet for the QCSEE engine must meet the design goals of providing a relatively large amount of inlet noise suppression with acceptable low-speed aerodynamic performance over the entire operating envelope, including a free-stream velocity of 41 meters per second at an angle of attack of 50° and in an 18-meter-per-second, 90° crosswind. The inlet noise-suppression goal led to the consideration of two basic inlet design concepts: The primary inlet design is referred to as the high-Mach-number inlet and the secondary design, as the low-Mach-number inlet. The low-Mach-number inlet design concept was considered as a backup should the relatively new high-Mach-number inlet concept not provide a satisfactory level of acoustic or aerodynamic performance. The

two inlet concepts are shown in figure 4(a), inlet nomenclature is defined in figure 4(b), and the inlet design parameters for both inlet concepts are listed in table I.

The high-Mach-number inlet has a design throat Mach number of 0.79 and uses the high-throat-Mach-number suppression concept (refs. 2 and 3) to provide inlet noise suppression during takeoff and approach. The inlet internal-lip-area contraction ratio $\left(D_{hl}/D_t\right)^2$ of 1.46 was selected to provide separation-free, high-angle-of-attack performance. The selection was based on the test results reported in reference 6. The internal lip shape is elliptic, with a major- to minor-axis ratio of 2.0. The inlet diffuser is a cubic shape, with a maximum wall angle of 8.7° occurring halfway down the diffuser. The external forebody has a DAC-1 contour and was designed for a drag-rise Mach number of approximately 0.79. The overall ratio of inlet length to fan diameter is 1.029.

The low-Mach-number inlet concept has a design throat Mach number of 0.60 and, in this case, inlet noise suppression is provided by acoustic treatment on the inlet diffuser walls. The internal lip has the same geometric parameter values as those for the high-Mach-number inlet. The diffuser section of the low-Mach-number inlet is a cubic shape with a maximum wall angle of 8.7° and is followed by a straight, cylindrical section. The cylindrical section is needed to provide the required surface area for acoustical treatment. The external forebody has the same DAC-1 contour as the high-Mach-number inlet with the same drag divergence Mach number of 0.79. The overall ratio of inlet length to fan diameter is 1.035.

The centerbody used with both inlets was designed to be compatible with this particular fan design. Its design parameters are given in table I. It is not the same centerbody design that is used with the QCSEE engine.

Both inlet concepts were tested with hard-wall diffusers and with a number of acoustically treated diffusers. Acoustic treatment is required with the high-Mach-number inlet to provide inlet noise suppression when the QCSEE engine is operating in reverse thrust. Three treatment designs were tested and the important design parameters of each are given in table II. The four high-Mach-number inlet configurations (one hard-wall and three treated diffusers) are designated as HM0, HM3.6, HM9.2, and HM24, where the HM refers to high Mach number and the 0, 3.6, 9.2, and 24 refer to the porosity (in percent) of the treatment face sheet. The investigation reported in references 4 and 5 had led to the selection of the HM9.2 inlet as the most promising for the QCSEE engine from an acoustic performance standpoint.

Four low-Mach-number inlet diffuser designs were also tested: a hard-wall design, LM0; and three treated designs, LM10, LM10mod, and LM28. The LM10mod configuration is a modified version of the LM10 configuration in which the most forward section of acoustical treatment is taped over (hard wall). In the low-Mach-number inlet noise suppression is provided by the acoustic treatment at takeoff, approach, and reverse thrust.

Instrumentation

Aerodynamic. - The aerodynamic instrumentation is shown in figure 5. Inlet performance was evaluated by means of 58 static-pressure taps on the inlet internal surfaces and a six-spoke total-pressure rake measuring a total of 114 total pressures at the inlet diffuser exit or fan face. Five rakes with six total-pressure probes and one thermocouple per rake were located downstream of the fan stators. Total-pressure and thermocouple probes were also located in the turbine discharge. At the muffler exit, 10 total-pressure and 10 total-temperature measurements were made.

Monitoring. - The instrumentation used to monitor the operation of the model is shown in figure 6. Strain gages were mounted on the fan blades, the turbine blades, and the fan-face rakes to monitor stress levels in those critical components. Accelerometers were mounted in various locations to monitor rig vibration levels. Proximity probes were located near the front bearing and midshaft to indicate the amount of shaft orbit.

To prevent possible high fan-blade stress levels, it was considered important that inlet internal flow separation be avoided as angle of attack was increased. To detect inlet flow separation, the pressure measurements p_l and $P_{180^o} - P_{0^o}$ (fig. 6) were continuously monitored as inlet angle of attack was increased. The onset of inlet flow separation is detected as a sudden increase in the values of p_l and $P_{180^o} - P_{0^o}$. This technique for detecting inlet flow separation is detailed in reference 9.

PROCEDURE

On-Line Data

As part of the test procedure, a number of on-line displays were used to insure safe operation of the model fan and to evaluate the data as they were being taken. Figure 7 shows three typical displays. Real-time frequency analysis of the fan-blade stress level was monitored on an oscilloscope display (fig. 7(a)). On the display were marked the stress limits for each resonant frequency mode of blade vibration (first bending, second bending, first torsion, etc.). This display provided a continuous status report on the stress level and also the resonant mode of any fan-blade vibration.

The onset of inlet internal flow separation was monitored on an x-y-y plotter (fig. 7(b)) with p_l and $P_{180^o} - P_{0^o}$ (fig. 6) on the two y-axes and angle of attack α on the x-axis. At a given free-stream velocity and fan speed, as angle of attack was increased the value of p_l decreased continuously (the lower lip surface velocity increased) while $P_{180^o} - P_{0^o}$ remain constant (any tip total-pressure loss remains circumferentially uniform). When inlet flow separation occurred, the values of p_l and

$P_{180^o} - P_{0^o}$ increased suddenly as illustrated in the figure. During the course of this test program, inlet flow separation was encountered with only one of the eight inlet configurations. This flow separation detection method allowed the model operator to immediately change the test condition (decrease angle of attack) in order to avoid prolonged operation at that condition.

After a test condition had been set and a data scan completed, a control panel oscilloscope display (fig. 7(c)) presented one line of output showing 10 of the most important items of reduced data from the digital data analysis computer. The test conductor could then examine the one line of information, determine whether or not he had gotten the desired data, and then make a decision as to what the next set point should be. Because as many as 16 data points accumulated on the scope display, the latest data scan could be compared with those taken previously.

Inlet Weight-Flow Measurement

Inlet weight flow (and hence throat Mach number) was determined by the method outlined in figure 8. Before any inlet tests, a standard bellmouth calibration inlet was installed for weight-flow calibration purposes (fig. 8(a)). After the variable-position muffler-exit plug was set at a given position and data were taken over the complete fan-speed range, one of the calibration curves shown in figure 8(b) could be constructed. The calibration curve represents the relation between the calculated muffler-exit corrected weight flow $(\dot{w}\sqrt{\theta}/\delta)_{muff}$ and the measured muffler-exit pressure conditions $(\Delta P/P)_{muff}$. The muffler corrected weight flow was determined from the sum of the fan weight flow measured by the bellmouth and the turbine weight flow measured by a supply-line venturi and from the measured muffler-exit total pressure and total temperature. This procedure was repeated for a number of plug positions, resulting in the family of curves shown schematically in figure 8(b). The actual calibration curves are shown in figure 9.

When an inlet was tested, the inlet weight flow was determined by the method outlined in figure 8(c). From the calibration curves, the plug position, and the measured muffler-exit conditions, the muffler-exit weight flow could be calculated. Then the turbine weight flow measured by the supply-line venturi could be subtracted from the total muffler-exit weight flow to get the inlet weight flow. Inlet throat Mach number was then calculated from the inlet weight flow, the free-stream total pressure and temperature, and the inlet geometric throat area.

Typical results of this inlet throat Mach number calculational procedure are given in table III. Data are shown for four combinations of free-stream velocity V_0, angle of attack α, and plug position x_{plug}. The first parameter listed in the table is $(\Delta P/P)_{0.3}$. This parameter is defined as the free-stream total pressure minus the inlet

internal-surface static pressure on the side of the inlet 30 percent of the way down from the highlight divided by the free-stream total pressure. This parameter should correlate directly with inlet weight flow and also be independent of free-stream velocity and angle of attack because the static pressure is measured far enough down the inlet duct and on the side of the duct. The fact that $(\Delta P/P)_{0.3}$ is nearly constant for the four conditions given in table III indicates that the calculated weight flow and throat Mach number should be the same for each of those conditions. As indicated by the final column in the table, the inlet throat Mach number that results from the weight flow calculated by using the muffler flow calibration techniques varies from 0.619 to 0.635. If the first condition in the table is not used in the comparison (since its value of $(\Delta P/P)_{0.3}$ is somewhat lower than those for the other three conditions), the Mach number variation is then from 0.626 to 0.635. This represents a variation in weight flow of about 0.93 percent.

Model Fan Operation

Details of the model fan design are given in reference 10. The fan stage has 15 rotor blades and 25 stator vanes. At the fan design rotational speed of 8020 rpm, the fan tip speed is 213.5 meters per second and the fan pressure ratio is about 1.17 for the operating lines used in this investigation.

The operating map for the fan is shown in figure 10. Two operating lines are shown in the figure: one for static conditions and one for free-stream velocities of 41 and 62 meters per second. The operating lines are different because of the change in wind tunnel static pressure (and hence fan backpressure) as free-stream velocity is changed. The operating lines for free-stream velocities of 0 and 41 meters per second were obtained with the muffler-exit plug in the same fixed position. The operating line for a free-stream velocity of 62 meters per second was made to coincide with that for 41 meters per second by moving the exit plug in to reduce the muffler-exit area by the required amount.

Test Procedure

In setting test conditions, inlet throat Mach number was based on a correlation between throat Mach number and an inlet weight-flow control parameter. This parameter is defined as free-stream total pressure minus an internal-surface static pressure at a given axial position on the side of the inlet ($\psi = 90^{\circ}$) divided by free-stream total pressure, $(P_0 - p_{x/L})/P_0$. (For the high-Mach-number inlets, $x/L = 0.4$; for the low-Mach-number inlets, $x/L = 0.3$.) The test procedure was then (1) to set free-stream velocity, (2) to set inlet throat Mach number by correlation with $(P_0 - p_{x/L})/P_0$, and (3) to set

angle of attack. Data were taken at this set point and then angle of attack was changed to the next value. After data were obtained over the range in angle of attack, inlet throat Mach number was changed and data were taken again over the range in angle of attack. After data had been taken over the complete range of inlet throat Mach number, the free-stream velocity was changed and the entire procedure was repeated. Data were taken at free-stream velocities of 0, 41, and 62 meters per second; angles of attack of 0°, 15°, 30°, 40°, and 50°; and inlet throat Mach numbers of 0.33, 0.45, 0.58, 0.72, 0.76, 0.79, and 0.82 for the high-Mach-number inlets and 0.30, 0.40, 0.50, 0.60, and 0.62 for the low Mach-number-inlets.

RESULTS AND DISCUSSION

Comparison of Inlets

Basic aerodynamic performance. - The basic aerodynamic performance of the four low-Mach-number and the four high-Mach-number inlet configurations is presented in table IV. In both cases, data are for the design throat Mach number (0.60 for the low-Mach-number inlets and 0.79 for the high-Mach-number inlets), for a free-stream velocity of 41 meters per second, and for angles of attack of 0° and 50°. The parameters presented are inlet total-pressure recovery $P_{1,av}/P_0$ and two total-pressure-distortion parameters, D_{max} and D_{60} (see symbol list for definitions).

For the low-Mach-number inlet configurations (table IV(a)), there was very little difference in the total-pressure recovery and just a slight increase in total-pressure distortion at a given angle of attack as the diffuser face-sheet porosity increased. Increasing the angle of attack from 0° to 50° resulted in a slight increase in the total-pressure-distortion parameters, but the inlet recovery remained essentially unchanged.

For the high-Mach-number inlet configurations (table IV(b)), the same trend was noted as for the low-Mach-number inlets - very little difference in total-pressure recovery and just a slight increase in the total-pressure-distortion parameter as the diffuser face-sheet porosity increased for a given angle of attack. Increasing the angle of attack from 0° to 50° resulted in more of a decrease in recovery and more of an increase in distortion than it did for the low-Mach-number inlets. For example, for the HM9.2 inlet configuration at an angle of attack of 0°, the recovery was 0.994 and the distortion D_{max} was 0.025. At an angle of attack of 50°, the recovery had decreased to 0.991 and the distortion had increased to 0.084.

Data obtained for all the inlet configurations at the other free-stream velocities (0 and 62 m/sec), the intermediate angles of attack (15°, 30°, and 40°), and other inlet throat Mach numbers show these same general trends. Details of the effects of free-stream velocity, throat Mach number, and angle of attack are presented in a later discussion of the HM9.2 inlet configuration.

Effect of diffuser face-sheet porosity on boundary-layer characteristics. - Details of the total-pressure distribution within the inlet boundary layer at the outer wall are shown in figure 11(a) for the low-Mach-number inlet configurations and in figure 11(b) for the high-Mach-number inlet configurations. The data are for a free-stream velocity of 41 meters per second, an angle of attack of 0°, and the design throat Mach number. The data are presented as the ratio of local to free-stream total pressure versus the fraction of passage height measured from the inlet outer wall at the diffuser exit.

The data for the low-Mach-number inlet configurations (fig. 11(a)) indicate a progressive increase in total-pressure loss at each measuring station in the boundary layer as diffuser face-sheet porosity was increased from 0 percent (LM0) to 28 percent (LM28). Taping over one section of the LM10 diffuser face sheet to make the LM10mod configuration slightly increased the local total-pressure ratio in the boundary layer because of the reduction in the amount of porous surface area. Hence, although the effect of increasing diffuser face-sheet porosity is not detectable in the overall inlet total-pressure recovery (tabulated for reference in fig. 11), the effect can be detected in the details of the boundary-layer measurements.

For the high-Mach-number inlets (fig. 11(b)), the results are similar: as face-sheet porosity was progressively increased from configuration HM0 to HM24, the local total-pressure ratio at each measuring station in the boundary layer decreased.

Although data are not shown, this same effect of increasing diffuser face-sheet porosity was also evident at all other conditions of free-stream velocity, angle of attack, and inlet throat Mach number for both low- and high-Mach-number inlet configurations.

Inlet flow separation. - All the inlet configurations were tested at angles of attack to 50° at a free-stream velocity of 41 meters per second. Only one configuration, HM24, experienced inlet flow separation within this angle of attack range. The results are shown in figure 12. The inlet flow separation detection traces that were discussed in the PROCEDURE section are shown for inlet throat Mach numbers of 0.76, 0.79, and 0.81. At a throat Mach number of 0.76 (fig. 12(a)), the inlet flow remained attached to an angle of attack of 50°, as evident from the continuous drop in lip static pressure p_{ℓ} and the constant level of diffuser-exit total-pressure difference $P_{180^{\circ}} - P_{0^{\circ}}$ as angle of attack was increased. At a throat Mach number of 0.79 (fig. 12(b)), and at an angle of attack of 50° the inlet flow had separated, as indicated by the sudden increase in p_{ℓ} and decrease in $P_{180^{\circ}} - P_{0^{\circ}}$. At the first indication of this separation, the angle of attack was decreased immediately and resulted in the return trace indicated by the arrows in figure 12(b). Flow separation was again encountered at a throat Mach number of 0.81 as indicated in figure 12(c).

Thus, the combination of high diffuser face-sheet porosity and high inlet throat Mach number (and hence a high diffusion rate) can lead to inlet flow separation at a lower angle of attack. A high diffuser face-sheet porosity by itself may not be enough to result in early inlet flow separation, as evident from the fact that the LM28 inlet con-

figuration (28-percent porosity) maintained attached flow to at least a 50° angle of attack. Also, a high throat Mach number (high diffusion rate) by itself may not result in early inlet flow separation as evident from the HM0, HM3.6, and HM9.2 configurations where the flow remained attached to at least a 50° angle of attack. It is the combination of both high diffuser face-sheet porosity and high inlet-throat Mach number that in this case had led to inlet flow separation at a 50° angle of attack. Also, since flow separation was not encountered with any of the other three high-Mach-number inlet configurations (which all had the same inlet lip design), it can be concluded that the flow separation of the HM24 inlet begins in the inlet diffuser.

As a reference point, the flow separation angle was 68° for a 30.48-centimeter-diameter inlet of the same geometric design as the HM0 inlet (hard-wall diffuser) at a free-stream velocity of 41 meters per second and a throat Mach number of 0.79 (ref. 6).

High-Mach-Number, 9.2-Percent-Porosity Inlet (HM9.2)

As already mentioned, the acoustic investigation reported in references 4 and 5 led to the selection of the HM9.2 inlet configuration as the primary candidate for the QCSEE engine. The aerodynamic results presented to this point have shown that this inlet performs well and that, from a low-speed aerodynamics standpoint, it is a good selection for the QCSEE engine. Therefore, the remainder of this discussion will concern further details of the aerodynamic performance of the HM9.2 inlet configuration.

Basic aerodynamic performance. - Figure 13 presents the basic aerodynamic performance of the HM9.2 inlet in terms of total-pressure recovery and distortion versus throat Mach number for constant angles of attack. For the static performance (fig. 13(a)) to a throat Mach number of 0.814, the total-pressure recovery was always above 0.991 and the distortion was always below 0.06. At a free-stream velocity of 41 meters per second and angles of attack of 0° to 50° (fig. 13(b)), distortion progressively increased and recovery decreased as angle of attack was increased at any throat Mach number. At the design throat Mach number of 0.79 and an angle of attack of 50° the total-pressure recovery was 0.991 and the total-pressure distortion D_{max} was 0.084. At a free-stream velocity of 62 meters per second (fig. 13(c)), the progressive effect of increasing angle of attack is again evident.

Boundary-layer characteristics. - The effect of increasing throat Mach number on the total-pressure distribution in the boundary layer at the diffuser exit for the HM9.2 inlet is shown in figure 14 at a free-stream velocity of 41 meters per second and an angle of attack of 0°. The data are plotted as the ratio of local to free-stream total pressure versus the fraction of the passage height measured from the outer wall. As would be expected, as the throat Mach number is increased (and hence surface velocities are increased) the total pressure decreases at any location in the tip boundary

layer. This accounts for the decrease in recovery and increase in distortion shown in figure 13.

The effect of increasing angle of attack on the total-pressure distribution in the tip boundary layer is shown in figure 15 at the design throat Mach number of 0.79 and a free-stream velocity of 41 meters per second. Data are shown for angles of attack of 0°, 30°, and 50° and at circumferential positions of 0° (windward), 60°, 120°, and 180° (leeward). The data indicate an increase in total-pressure loss in the boundary layer on the windward side of the inlet and a slight decrease in total-pressure loss on the leeward side as angle of attack is increased to 50°. This behavior, which is described in the following section is a result of the increase in surface velocities on the windward side and the decrease in surface velocities on the leeward side as angle of attack is increased.

Surface pressure distributions. - The axial distribution of surface static pressure is shown in figure 16 as angle of attack was increased from 0° to 50° at a free-stream velocity of 41 meters per second and the design throat Mach number of 0.79. The data are plotted as the ratio of surface static to free-stream total pressure versus the fraction of the inlet length measured from the highlight. In figure 16(a), surface static-pressure distributions on the windward side ($\psi = 0^{\circ}$) are shown for angles of attack of 0°, 30°, 40°, and 50°. As angle of attack was increased, surface static pressure progressively decreased (surface velocity increased) from the highlight back to about 35 percent of the inlet length. At angles of attack of 40° and 50°, the surface static pressure at first increased and then decreased just downstream of the highlight, indicating the possible formation of a flow separation bubble on the inlet lip (ref. 11).

On the leeward side ($\psi = 180^{\circ}$, fig. 16(b)) the effect of increasing angle of attack is just opposite to what it was on the windward side. As angle of attack was increased, the surface static pressure on the leeward side increased (surface velocity decreased from 0° to 50°) from the highlight back to about 35 percent of the inlet length. These changes in surface velocity on the windward and leeward sides of the inlet as angle of attack was increased explain the corresponding changes in total-pressure loss discussed in the preceding section.

Evaluation of throat Mach number control parameter. - As was mentioned in the INTRODUCTION, with a high-Mach-number inlet concept like the HM9.2, relatively large changes in inlet throat Mach number (and hence noise suppression) can occur with smaller changes in inlet airflow. Therefore, maintaining a constant level of noise suppression with this inlet concept requires that the QCSEE engine control engine weight flow quite accurately under changing conditions of free-stream velocity and angle of attack. Reference 3 reports that an effective control parameter for maintaining constant inlet throat Mach number is the ratio of inlet diffuser surface static pressure to free-stream total pressure. The surface static pressure was measured far downstream in the diffuser and also on the side walls of the diffuser in order to eliminate any effect of changes in free-stream velocity and angle of attack on the one-to-one relation between

the control parameter and the throat Mach number.

The location of the diffuser surface static-pressure measurement for the QCSEE inlet control parameter was selected to be 40 percent of the inlet length downstream of the highlight (fig. 17). The effectiveness of the control parameter is also shown in figure 17, where inlet throat Mach number is plotted against the control parameter for angles of attack from 0° to 50°. The correlation between the two quantities remained nearly unchanged as angle of attack was increased to 30° (the maximum angle to which the inlet is required to perform well acoustically). A solid line has been drawn through the 0°-angle-of-attack data points and a dashed line through the 30° data points to better illustrate the correlation. Therefore, if a constant value of the weight-flow control parameter is maintained, the inlet Mach number will remain constant, and hence the inlet noise suppression will remain constant, as inlet angle of attack is increased to the maximum acoustical design value of 30°.

Scale Effects

One of the inlets tested during the investigation reported in reference 6 was of the same geometric design as the HM0 inlet (both having hard-wall diffusers). The inlet of reference 6 had a 30.48-centimeter diffuser-exit diameter; the HM0 inlet had a 50.80-centimeter diffuser-exit diameter. Hence an appreciation for the effects of inlet scale can be gained by comparing results for the two inlets.

Inlet total-pressure recovery for the two inlets is shown in figure 18 as a function of throat Mach number at a free-stream velocity of 41 meters per second and an angle of attack of 0°. The total-pressure recovery for the larger inlet is higher than that for the smaller inlet over the entire range of throat Mach number because boundary-layer thickness is a smaller percentage of the diffuser-exit flow area as the inlet scale is increased. (The exit area increased with an increase in diameter squared, but the boundary-layer thickness increased with an increase in inlet length to a power less than 1 (ref. 12).) This result suggests that the smaller the scale, the more pessimistic the results and that a full-scale inlet can be expected to perform better than a small-scale model.

The axial distribution of surface static- to free-stream total-pressure ratio for the two inlets is shown in figure 19 for angles of attack of 0° and 50°, the design throat Mach number of 0.79, and a free-stream velocity of 41 meters per second. The data agree very well over the length of the inlets at both angles of attack. This result was expected since, although the inlets are of different size, they are of the same geometric proportions.

SUMMARY OF RESULTS

Tests were conducted to determine the aerodynamic performance of inlets intended for use with the QCSEE engine. The main results of the investigation can be summarized as follows:

1. Increasing the inlet diffuser face-sheet porosity resulted in an increase in total-pressure loss in the tip boundary layer for both the high- and low-Mach-number inlets. However, the effect on overall inlet total-pressure recovery was insignificant.

2. The primary inlet intended for use with the QCSEE engine from an acoustic standpoint (high Mach number, 9.2-percent porosity) had a total-pressure recovery and a distortion of 0.991 and 0.084, respectively, at the design throat Mach number, a free-stream velocity of 41 meters per second, and an angle of attack of 50°. Inlet flow separation did not occur to at least a 50° angle of attack over the entire range of throat Mach number tested with this inlet.

3. The QCSEE inlet weight-flow control parameter related directly to inlet throat Mach number (and hence inlet noise suppression) with no significant effect of angle of attack to 30° (the acoustics requirement).

4. Inlet flow separation was encountered with only one inlet - the high-Mach-number inlet with 24-percent porosity. Separation occurred at an angle of attack of 50° with throat Mach numbers of 0.79 and 0.81 and a free-stream velocity of 41 meters per second. The separation angle of attack at these same conditions for a 30.48-centimeter-diameter inlet of the same geometric design, but with a hard-wall diffuser, was 68°. Hence a highly porous diffuser wall (as opposed to a hard-wall diffuser) in combination with a high inlet throat Mach number (high diffusion rate) can result in diffuser flow separation at a lower angle of attack.

5. Comparing data for 50.80- and 30.48-centimeter-diameter inlets (both high Mach number) indicated higher levels of total-pressure-recovery for the larger inlet. Internal surface pressure distributions for the two inlets were nearly identical.

Lewis Research Center,
National Aeronautics and Space Administration,
Cleveland, Ohio, April 14, 1978,
505-05.

REFERENCES

1. Albers, James A.: Predicted Upwash Angles at Engine Inlets for STOL Aircraft. NASA TM X-2593, 1972.

2. Abbott, J. M.: Aeroacoustic Performance of Scale Model Sonic Inlets. AIAA Paper 75-202, Jan. 1975.

3. Miller, B. A.: Experimentally Determined Aeroacoustic Performance and Control of Several Sonic Inlets. AIAA Paper 75-1184, Sept. 1975.

4. Bilwakesh, K. R.; and Clemons, A.: Acoustic Tests on a 20-Inch (50.8-cm) Diameter Scale Model (1:3.5) Fan and Inlet for the Under-the-Wing Engine, Vol. I. NASA CR-135117, 1978.

5. Bilwakesh, K. R.; and Clemons, A.: Acoustic Tests on a 20-Inch (50.8-cm) Diameter Scale Model (1:3.5) Fan and Inlet for the Under-the-Wing Engine, Vol. II. NASA CR-135118, 1978.

6. Miller, Brent A.; Dastoli, Benjamin J.; and Wesoky, Howard L.: Effect of Entry-Lip Design on Aerodynamics and Acoustics of High-Throat-Mach-Number Inlets for the Quiet, Clean, Short-Haul Experimental Engine. NASA TM X-3222, 1975.

7. Yuska, Joseph A.; Diedrich, James H.; and Clough, Nestor: Lewis 9- by 15-Foot V/STOL Wind Tunnel. NASA TM X-2305, 1971.

8. Dietrich, Donald A.; Heidmann, Marcus F.; and Abbott, John M.: Acoustic Signatures of a Model Fan in the NASA-Lewis Anechoic Wind Tunnel. AIAA Paper 77-59, Jan. 1977.

9. Luidens, Roger W.; and Abbott, John M.: Incidence Angle Bounds for Lip Flow Separation of Three 13.97-Centimeter-Diameter Inlets. NASA TM X-3351, 1976.

10. Lewis, G. W., Jr.; and Tysl, E. R.: Overall and Blade-Element Performance of a 1.20-Pressure-Ratio Fan Stage at Design Blade Setting Angle. NASA TM X-3101, 1974.

11. Jakubowski, A. K.; Luidens, R. W.: Internal Cowl-Separation at High Incidence Angles. AIAA Paper 75-64, Jan. 1975.

12. Schlichting, Hermann (J. Kestin, transl.): Boundary Layer Theory. Fourth ed. McGraw-Hill Book Co., Inc., 1960, p. 537.

TABLE I. - INLET GEOMETRIC PARAMETERS

Geometric variable	Low-Mach-number inlet	High-Mach-number inlet
Internal lip		
Contraction ratio, $(D_{hl}/D_t)^2$	1.46	1.46
Surface contour	Ellipse	Ellipse
Proportions, a/b	2.0	2.0
External forebody		
Diameter ratio, D_{hl}/D_{max}	0.880	0.900
Ratio of length to maximum diameter, C/D_{max}	0.310	0.219
Surface contour[a]	DAC-1	DAC-1
Proportions, c/d	5.166	4.380
Diffuser		
Ratio of exit flow area to inlet flow area, $\left(D_e^2 - D_c^2\right)/D_t^2$	1.011	1.156
Ratio of diffuser length to exit diameter, L_d/D_e	0.850	0.856
Maximum local wall angle, λ_{max}, deg	8.7	8.7
Location of maximum local wall angle, percent L_d	33.8	50
Equivalent conical half-angle, deg	0.17	2.08
Surface contour	Cubic	Cubic
Centerbody		
Ratio of length to diameter, L_c/D_c	0.935	0.935
Surface contour	NACA-1	NACA-1
Ratio of centerbody length to diffuser length, L_c/L_d	0.416	0.418
Ratio of centerbody diameter to diffuser-exit diameter, D_c/D_e	0.46	0.46
Overall		
Ratio of inlet length to diffuser-exit diameter, L/D_e	1.035	1.029

[a]The DAC-1 contour was developed by the Douglas Aircraft Co. and is given by $\left(\frac{y}{d}\right)^2 = 2.318\left(\frac{x}{c}\right) - 2.748\left(\frac{x}{c}\right)^2 + 2.544\left(\frac{x}{c}\right)^3 - 1.113\left(\frac{x}{c}\right)^4$.

TABLE II. - INLET DIFFUSER WALL TREATMENT DESIGNS

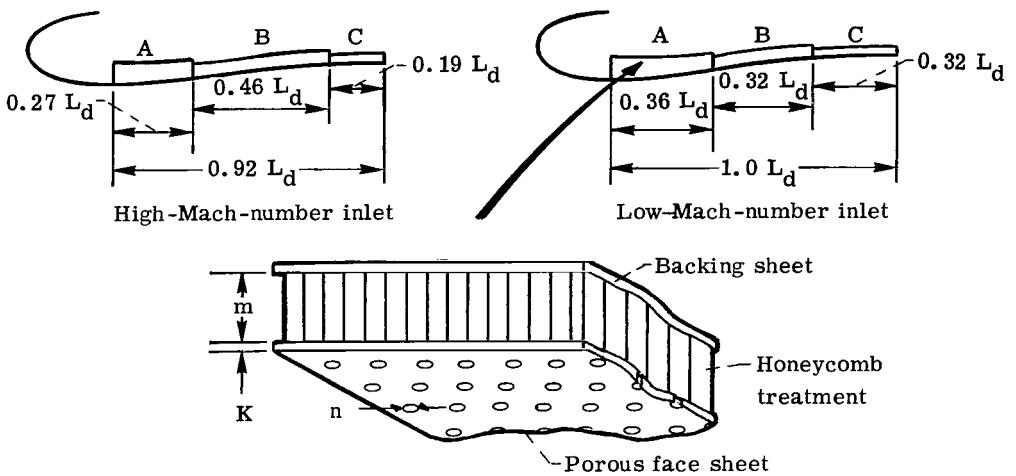

Inlet type	Inlet designation	Porosity, percent	Hole diameter, n, cm	Face-sheet thickness, K, cm	Backing depth, m, cm		
					A	B	C
High Mach number	HM0	0	0	------	----	-----	-----
	HM3.6	3.6	.158	0.0508	1.42	0.325	0.134
	HM9.2	9.2	.110	.0508	1.72	.57	.312
	HM24	24	.060	.081	1.72	.57	.312
Low Mach number	LM0	0	0	------	----	-----	-----
	LM10	10	.158	0.0508	1.42	0.381	0.147
	LM10mod	10	.158	.0508	----	.381	.147
	LM28	28	.114	.081	1.27	1.27	1.27

TABLE III. - TYPICAL RESULTS OF INLET THROAT MACH NUMBER CALCULATION PROCEDURE

Pressure parameter, $(\Delta P/P)_{0.3}$	Free-stream velocity, V_0	Angle of attack, α, deg	Muffler plug position, x_{plug}, cm	Muffler weight flow,[a] $\dot{w}_{muff}$, kg/sec	Simulator turbine weight flow, $\dot{w}_{turb}$, kg/sec	Inlet weight flow,[b] $\dot{w}_{inlet}$, kg/sec	Throat Mach number,[b] M_t
0.251	0	0	26.85	37.05	5.29	31.76	0.619
.255	43.01	0	27.99	37.12	5.14	31.98	.626
.257	41.65	50	27.99	37.26	5.14	32.12	.631
.255	63.89	0	25.44	37.50	5.22	32.28	.635

[a]Determined from curves of fig. 8(b).
[b]Determined from calculations of fig. 8(c).

TABLE IV. - AERODYNAMIC PERFORMANCE OF INLETS

[Free-stream velocity, V_0, 41 m/sec.]

(a) Low-Mach-number inlets; throat Mach number, M_t, 0.60

Inlet	Angle of attack, α, deg					
	0			50		
	Total-pressure recovery, $P_{1,av}/P_0$	Inlet total-pressure-distortion parameter, D_{max}	Inlet circumferential total-pressure-distortion parameter, D_{60}	Total-pressure recovery, $P_{1,av}/P_0$	Inlet total-pressure-distortion parameter, D_{max}	Inlet circumferential total-pressure-distortion parameter, D_{60}
LM0	0.996	0.005	0	0.995	0.035	0.004
LM10	.996	.005	↓	.995	.035	.003
LM10mod	.996	.009		-----	-----	-----
LM28	.994	.022		.993	.047	.004

(b) High-Mach-number inlets; throat Mach number, M_t, 0.79

HM0	0.994	0.027	0.002	0.992	0.073	0.008
HM3.6	.994	.023	.001	.991	.083	.009
HM9.2	.994	.025	.001	.991	.084	.008
HM24	.992	.046	.001	.989	.104	.010

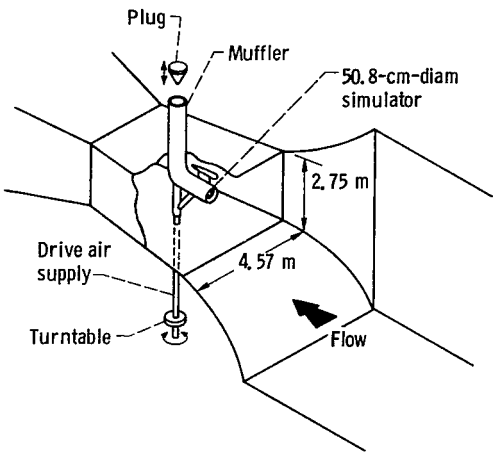

Figure 1. - Schematic of 9- by 15-Foot Low-Speed Wind Tunnel showing model installation.

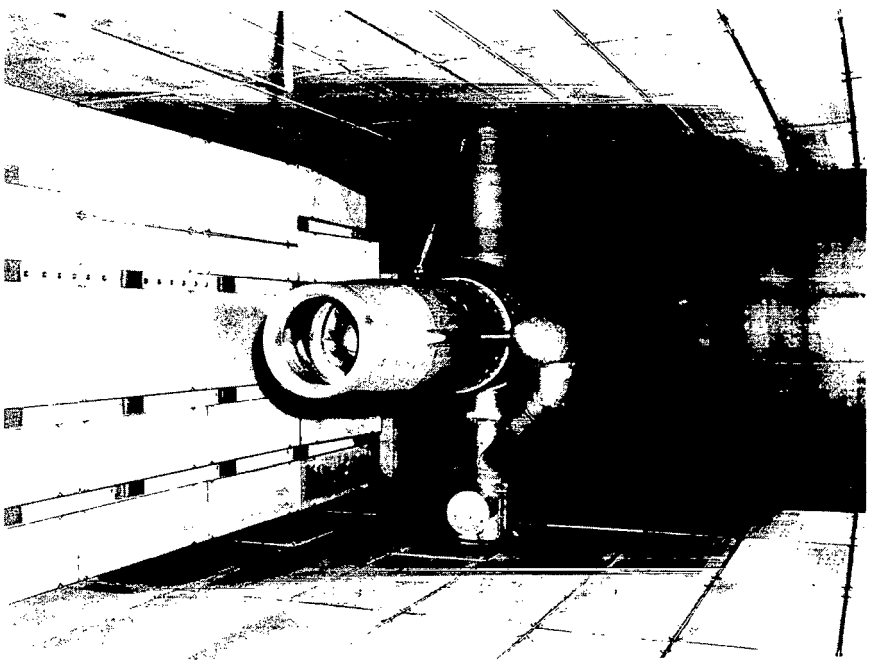

Figure 2. - Model installation in 9- by 15-Foot Low-Speed Wind Tunnel.

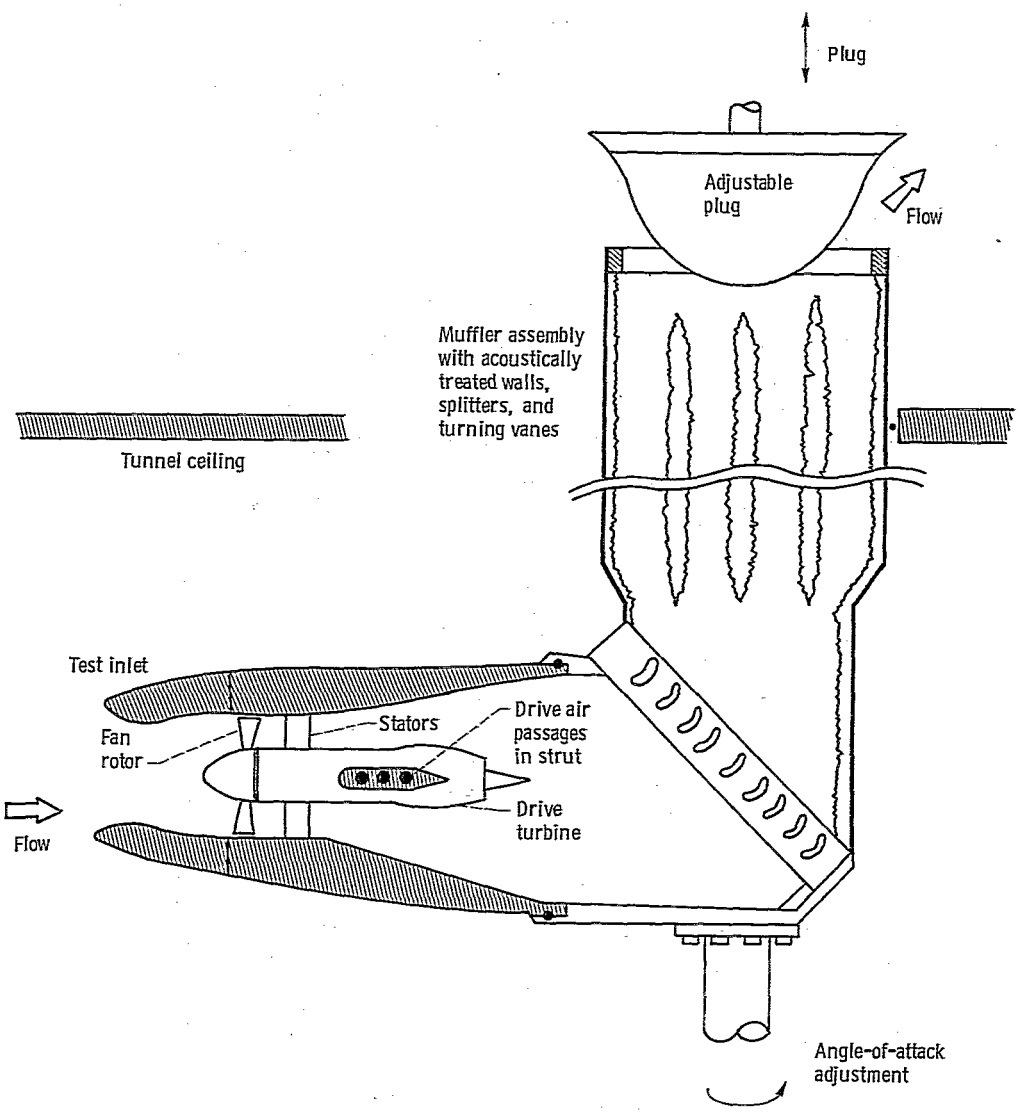

Figure 3. - General view of model and muffler.

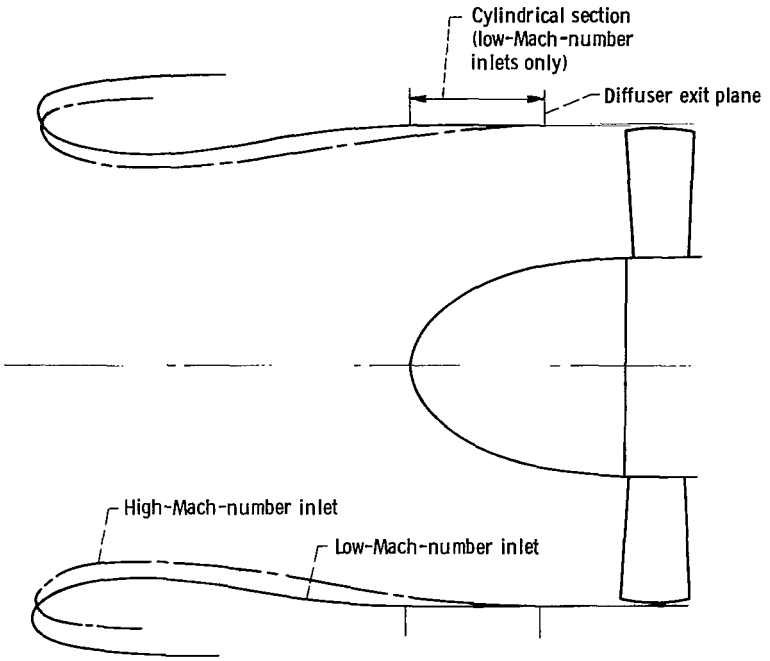

(a) Comparison of inlets.

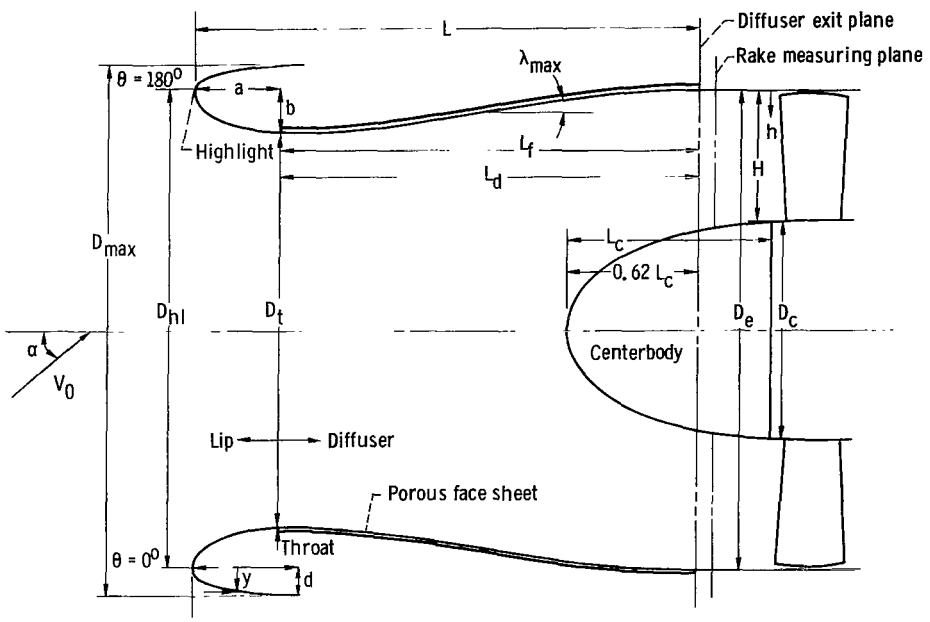

(b) Inlet nomenclature.

Figure 4. - Inlet designs.

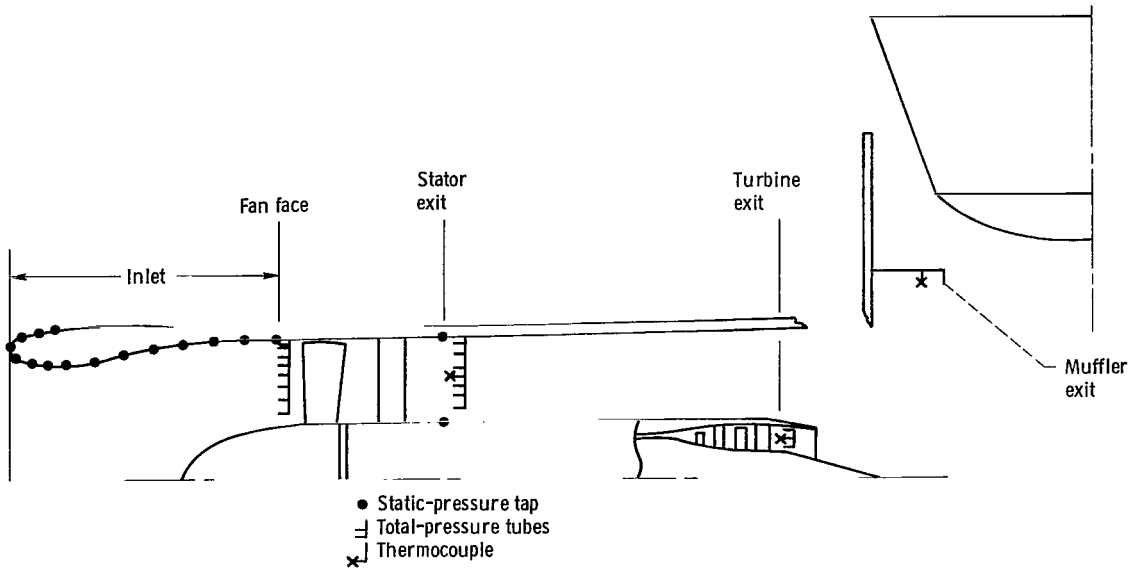

Region	Total-pressure tubes (rakes)	Static-pressure taps	Thermo-couples
Inlet	------	58	--
Fan face	114 (6)	6	--
Stator exit	30 (5)	10	5
Turbine exit	6 (4)	6	6
Muffler exit	10 (10)	--	10

Figure 5. - Model research instrumentation.

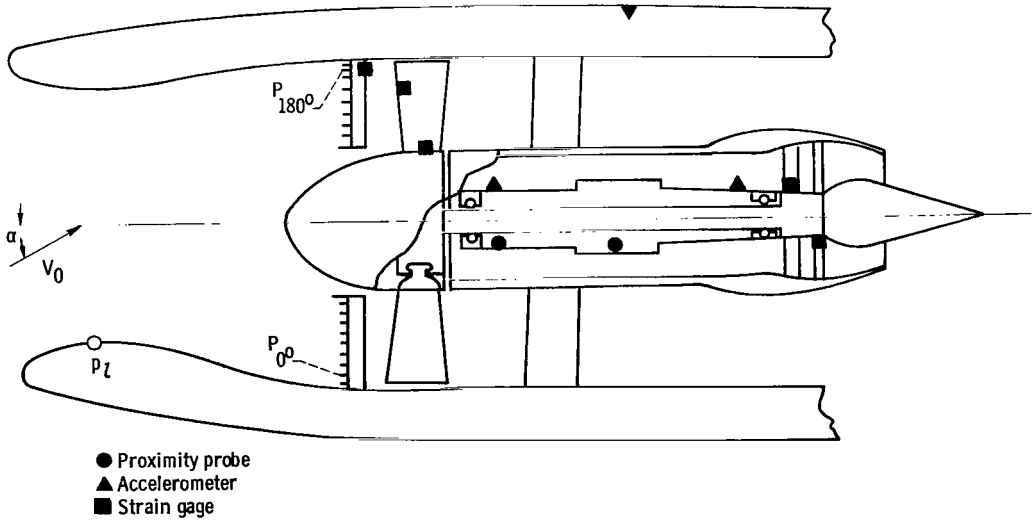

Figure 6. - Monitoring instrumentation.

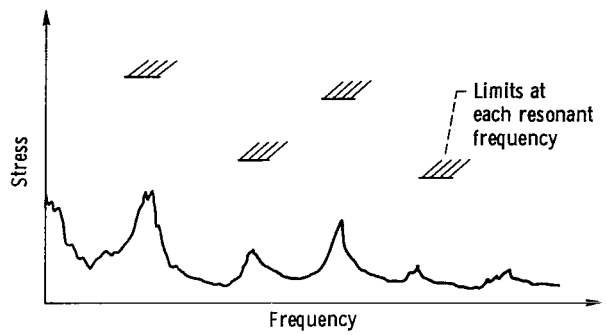

(a) Typical real-time spectrum analyzer display of fan-blade stress levels.

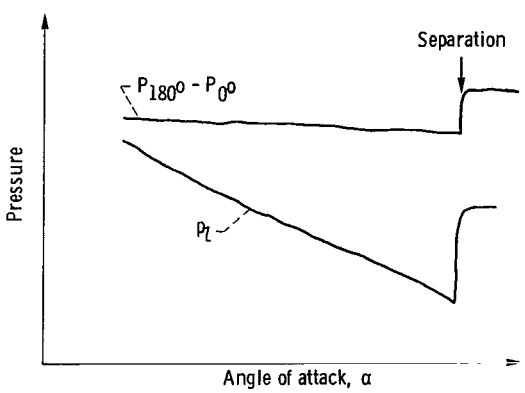

(b) Typical inlet flow separation monitor traces.

RDG	QR	ALPHA	RPM	%DSPD	WFMCT	MTHRT	ILTPP	PRECA	DISA2	FPRA
308	21.12	40.32	8542.	104.7	67.78	0.714	0.235	0.992	0.048	1.1839
309	21.09	50.39	8540.	104.7	67.46	0.706	0.236	0.992	0.058	1.1836
310	23.08	0.160	8854.	108.6	69.96	0.772	0.254	0.991	0.044	1.2008

(c) Typical display of model performance parameters from digital computer.

Figure 7. - On-line displays utilized during tests.

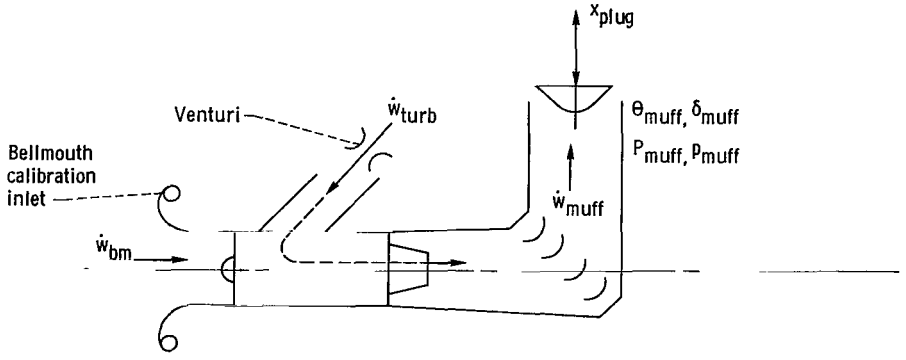

(a) Calibration setup.

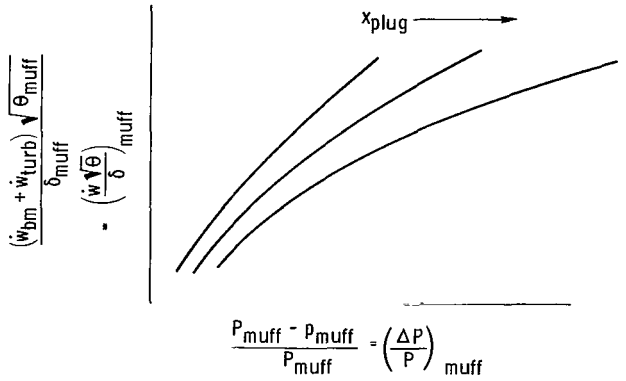

(b) Weight-flow calibration curves.

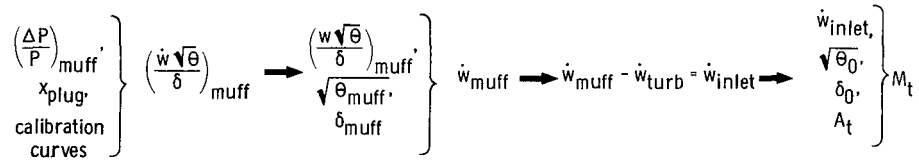

(c) Determination of throat Mach number during inlet tests.

Figure 8. - Weight flow calibration and calculation of inlet throat Mach number.

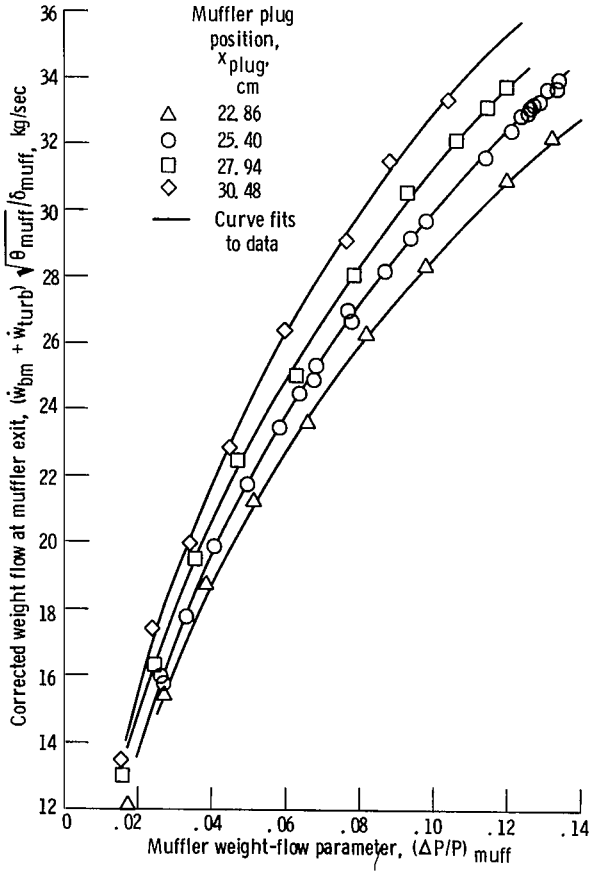

Figure 9. - Muffler weight-flow calibration.

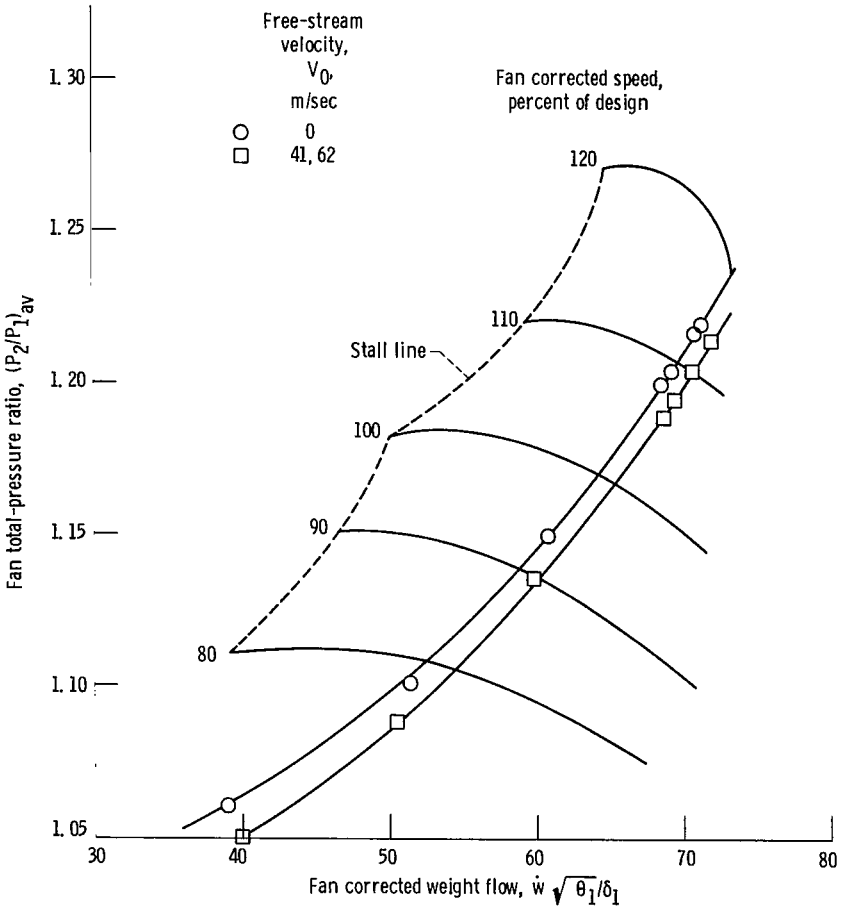

Figure 10. - Fan operating lines used during tests. (Speed lines from ref. 10.)

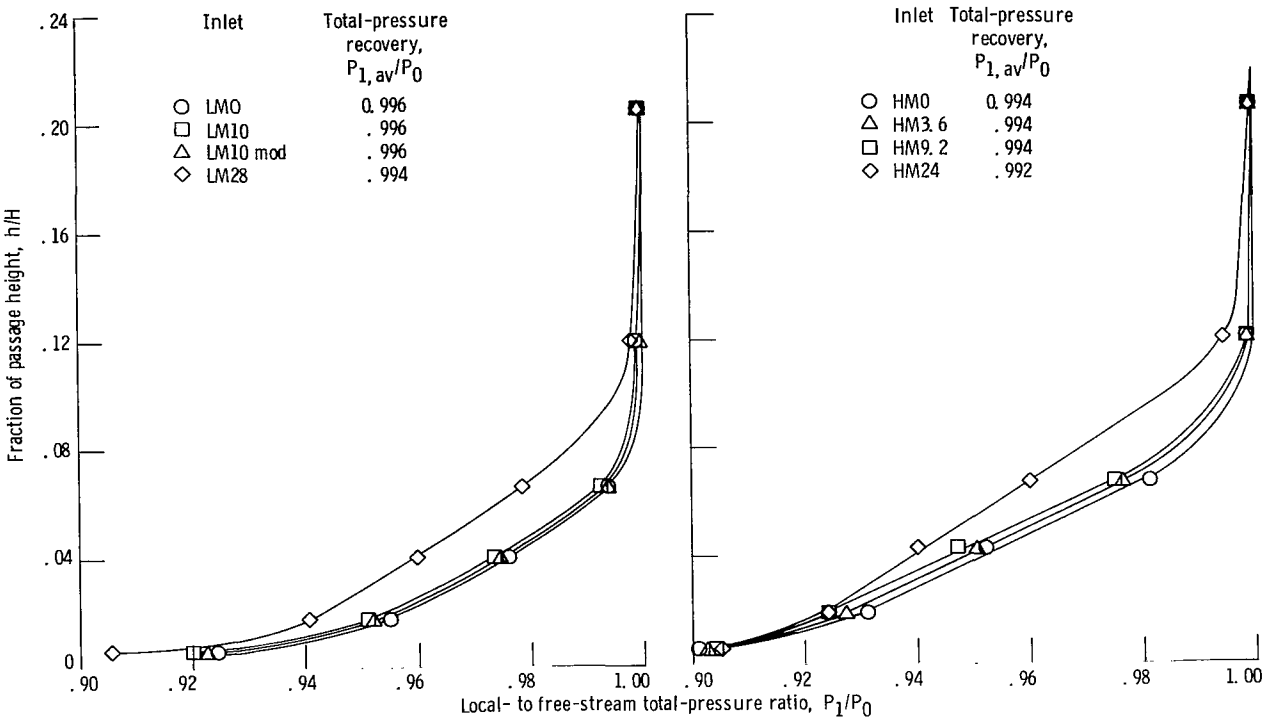

(a) Low-Mach-number inlets; throat Mach number, M_t, 0.60.

(b) High-Mach-number inlets; throat Mach number, M_t, 0.79.

Figure 11. - Local total-pressure ratio in tip boundary layer at inlet diffuser exit. Free-stream velocity, 41 meters per second. Angle of attack, α, 0^0.

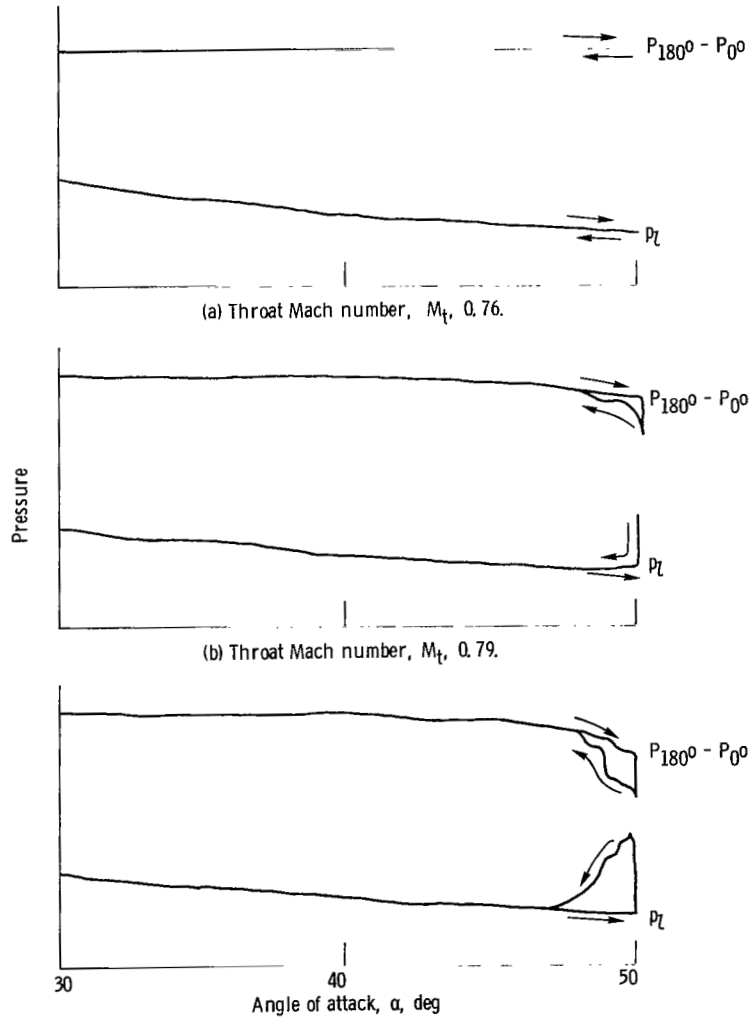

(a) Throat Mach number, M_t, 0.76.

(b) Throat Mach number, M_t, 0.79.

(c) Throat Mach number, M_t, 0.81.

Figure 12. - HM24 inlet flow separation. Free-stream velocity, V_0, 41 meters per second.

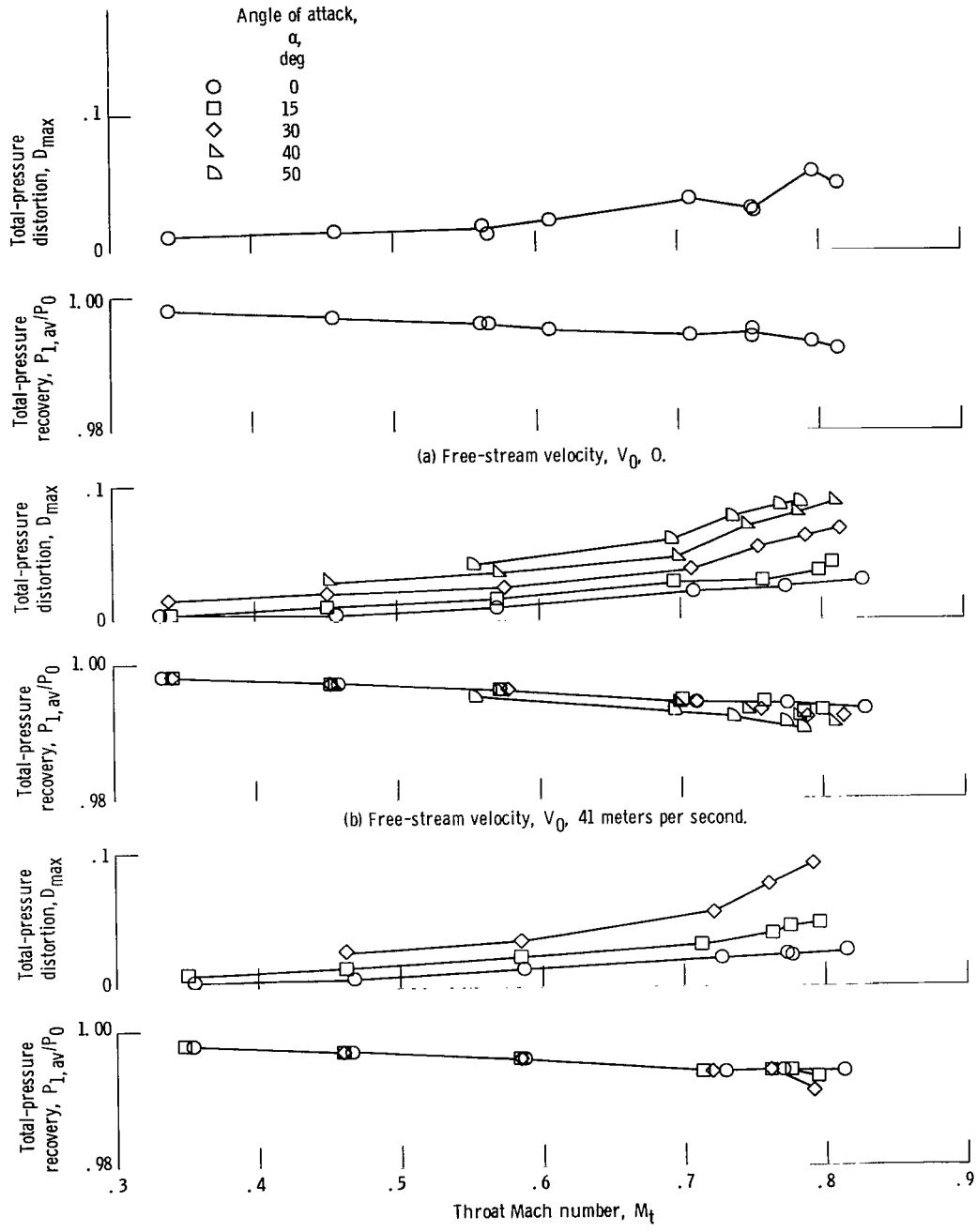

(a) Free-stream velocity, V_0, 0.

(b) Free-stream velocity, V_0, 41 meters per second.

(c) Free-stream velocity, V_0, 62 meters per second.

Figure 13. - Aerodynamic performance of HM9. 2 inlet.

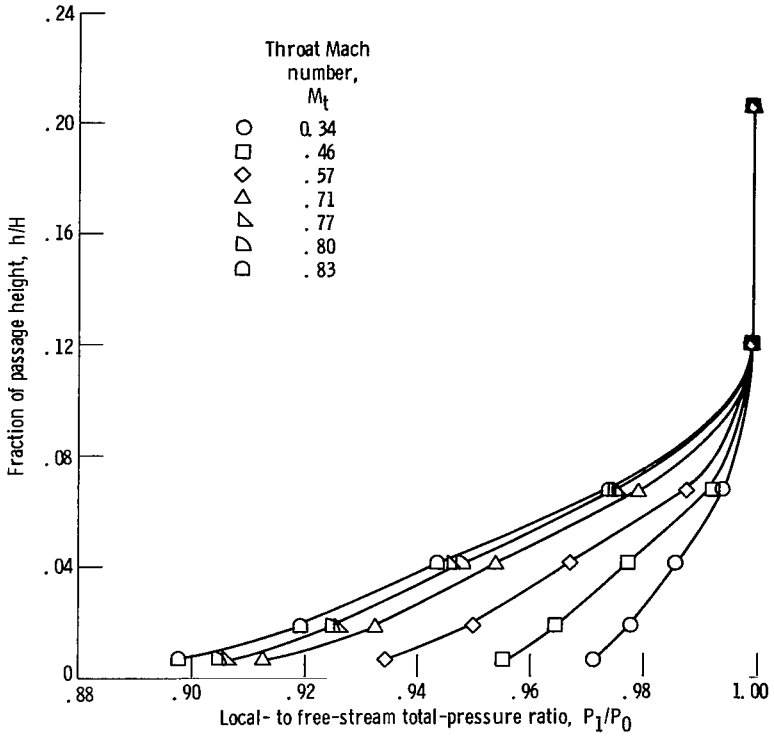

Figure 14. - Effect of inlet throat Mach number on local total-pressure ratio in tip boundary layer at inlet diffuser exit for HM9.2 inlet. Free-stream velocity, V_0, 41 meters per second; angle of attack, α, 0^0.

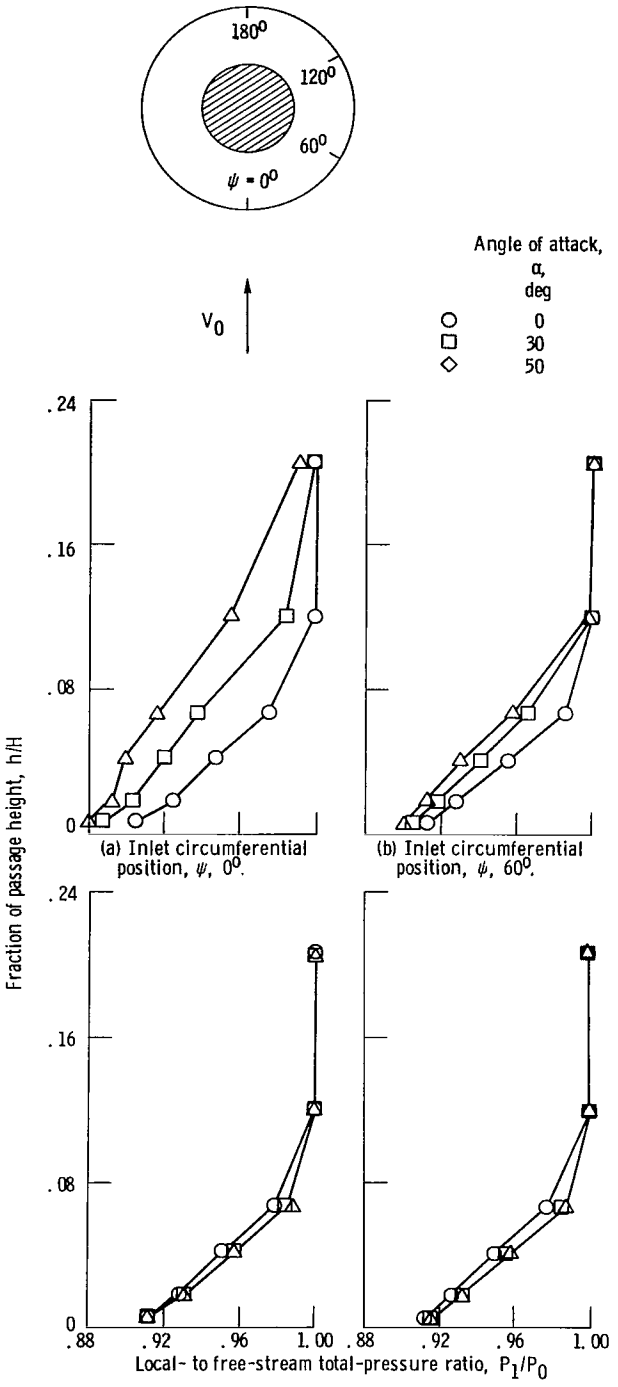

Figure 15. - Effect of angle of attack on local total-pressure ratio in tip boundary layer at inlet diffuser exit for HM9.2 inlet. Free-stream velocity, V_0, 41 meters per second; throat Mach number, M_t, 0.79.

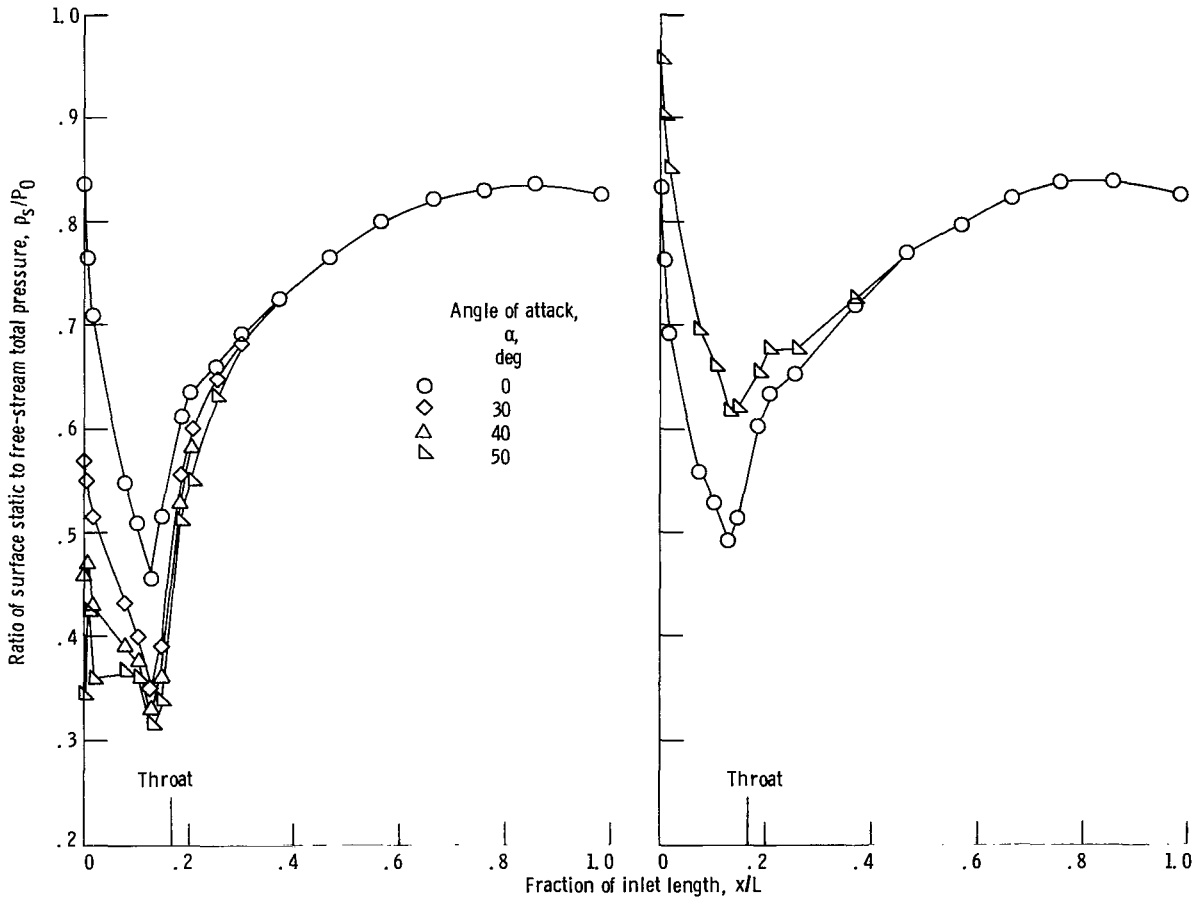

(a) Circumferential position, ψ, 0^0.

(b) Circumferential position, ψ, 200^0.

Figure 16. - Effect of angle of attack on axial distribution of surface static pressure for HM9.2 inlet. Free-stream velocity, V_0, 41 meters per second; throat Mach number, M_t, 0.79.

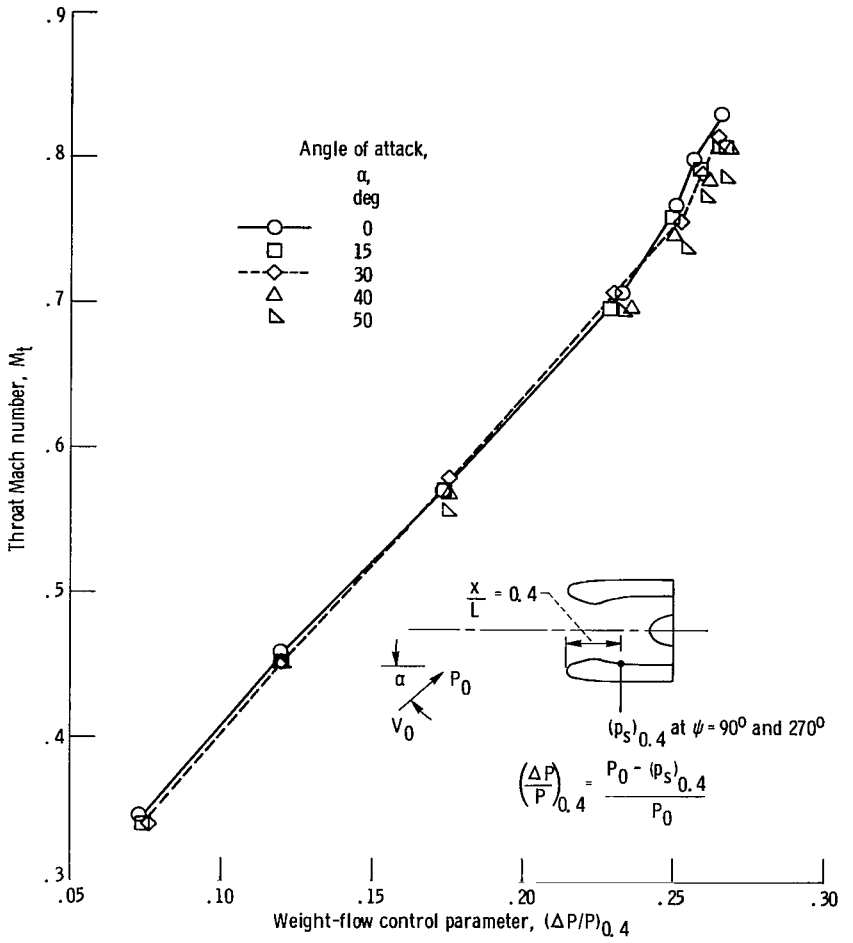

Figure 17. - Effect of angle of attack on relation between inlet throat Mach number and weight-flow control parameter for HM9.2 inlet. Free-stream velocity, V_0, 41 meters per second.

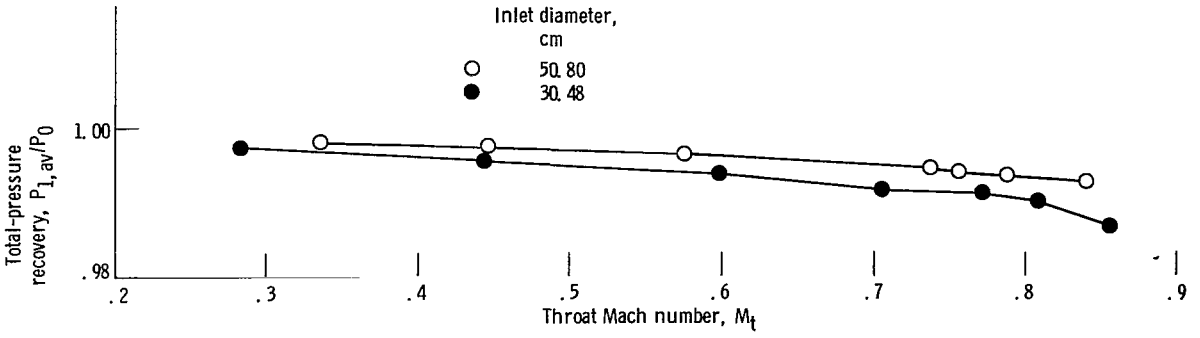

Figure 18. - Aerodynamic performance of 30.48- and 50.80-centimeter-diameter HMO inlets. Free-stream velocity, V_0, 41 meters per second; angle of attack, α, 0^0.

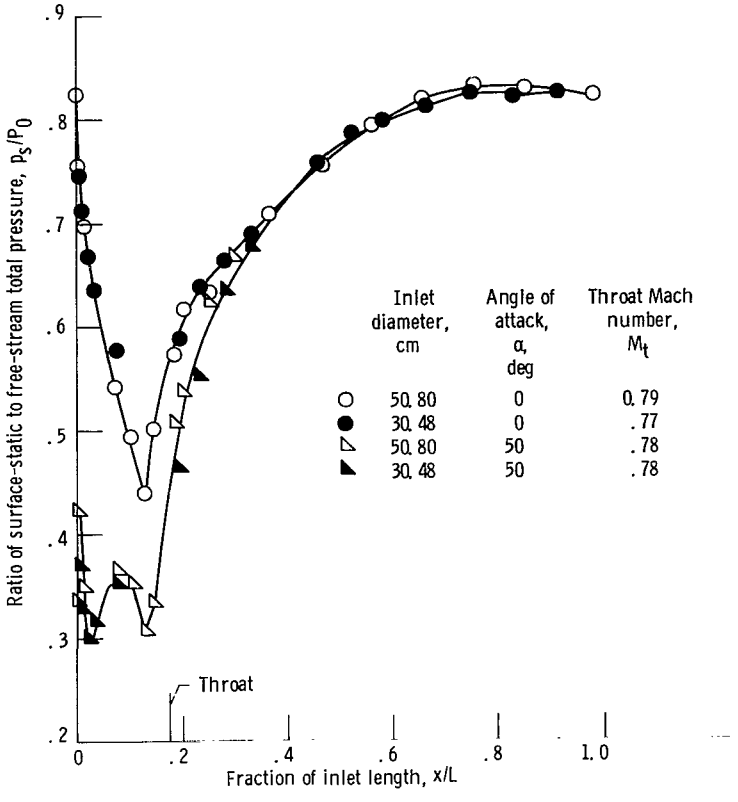

Figure 19. - Axial distribution of surface static pressure for 30.48- and 50.80-centimeter-diameter HMO inlets. Free-stream velocity, V_0, 41 meters per second.

1. Report No.	2. Government Accession No.	3. Recipient's Catalog No.
NASA TP-1178		

4. Title and Subtitle: LOW-SPEED AERODYNAMIC PERFORMANCE OF 50.8-CENTIMETER-DIAMETER NOISE-SUPPRESSING INLETS FOR THE QUIET, CLEAN, SHORT-HAUL EXPERIMENTAL ENGINE (QCSEE)

5. Report Date: August 1978

6. Performing Organization Code:

7. Author(s): John M. Abbott, James H. Diedrich, and Robert C. Williams

8. Performing Organization Report No.: E-9542

9. Performing Organization Name and Address:
National Aeronautics and Space Administration
Lewis Research Center
Cleveland, Ohio 44135

10. Work Unit No.: 505-05

11. Contract or Grant No.:

12. Sponsoring Agency Name and Address:
National Aeronautics and Space Administration
Washington, D. C. 20546

13. Type of Report and Period Covered: Technical Paper

14. Sponsoring Agency Code:

15. Supplementary Notes:

16. Abstract

A series of tests were conducted to determine the aerodynamic performance of inlets designed for the quiet, clean, short-haul, experimental engine (QCSEE). Two basic inlet concepts were tested - a high-throat-Mach-number (0.79) design and a low-throat-Mach-number (0.60) design. Both concepts were tested with four diffuser acoustical treatment designs that had face-sheet porosity ranging from 0 to 24 percent for the high-Mach-number inlet and 0 to 28 percent for the low-Mach-number inlet. The tests were conducted in a low-speed wind tunnel at free-stream velocities of 0, 41, and 62 m/sec and angles of attack to 50°. Inlet throat Mach number was varied about the design value. Increasing the inlet diffuser face-sheet porosity resulted in an increase in total-pressure loss in the boundary layer for both the high- and low-Mach-number inlet designs. However, the overall effect on inlet total-pressure recovery was insignificant. The primary inlet configuration intended for use with the QCSEE engine (high Mach number, 9.2-percent porosity) had a total-pressure recovery of 0.991 at the design throat Mach number, a free-stream velocity of 41 m/sec, and an angle of attack of 50°. Inlet flow separation at an angle of attack of 50° was encountered with only one inlet configuration - the high-Mach-number design with the highest diffuser face-sheet porosity (24 percent).

17. Key Words (Suggested by Author(s))	18. Distribution Statement
Inlet design; High throat Mach number inlet; Sonic inlet; Noise suppressing inlet; Acoustically treated inlet; Wind tunnel tests	Foreign distribution excluded. Source of Availability: NASA Industrial Applications Centers

19. Security Classif. (of this report)	20. Security Classif. (of this page)	21. No. of Pages	22. Price*
Unclassified	Unclassified	35	A03

"Available: NASA'S Industrial Application Centers"

NASA-Langley, 1978

National Aeronautics and
Space Administration

Washington, D.C.
20546

Official Business
Penalty for Private Use, $300

SPECIAL FOURTH CLASS MAIL
BOOK

Postage and Fees Paid
National Aeronautics and
Space Administration
NASA-451

NASA

POSTMASTER: If Undeliverable (Section 158
Postal Manual) Do Not Return